Proceedings of International Conference on
Technology and Social Science 2018 (ICTSS 2018)

Study on Multi-tone Signals for Design and Testing of Linear Circuits and Systems

Yukiko Shibasaki [1,a], Koji Asami [1,b], Anna Kuwana [1,c], Yuanyang Du [1,d], Akemi Hatta [1,e], Kazuyoshi Kubo [2,f] and Haruo Kobayashi [1,g]

[1]Division of Electronics and Informatics, Faculty of Science and Engineering, Gunma University

1-5-1 Tenjin-cho Kiryu, Gunma, Japan 376-8515

[2]Oyama National College of Technology, Oyama, Tochigi 323-0806 Japan

[a]<t15304056@gunma-u.ac.jp>, [b]<koji.asami@advantest.com>, [c]<kuwana.anna@gunma-u.ac.jp>, [d]<t171d602@gunma-u.ac.jp>, [e]<t15304096@gunma-u.ac.jp>, [f]<kubo@oyama-ct.ac.jp>, [g]<koba@gunma-u.ac.jp>

Keywords: Multi-tone signal, Cosine wave, Sine wave, Crest factor, Hilbert transform, Impulse signal

Abstract. This paper studies characteristics of multi-tone signals, for design and testing of linear circuits and systems. First, we show simulation results of three algorithms (Kitayoshi, Newman, Schroeder) for minimizing the crest factor in multi-tone signals and compare them. The crest factor is a measure of a waveform and defined as the peak amplitude of a waveform divided by the RMS value. For example, a sine wave has a crest factor of 1.414:1. A multi-tone signal minimizing the crest factor used for such high SNR measurement of the analog circuits can be realized by proper selection of the initial phases. We found from simulation results that the crest factor was the smallest at 1.661 (which is only 1.16 times larger than the sine wave) when using the Newman algorithm, even though the crest factor is almost comparable for the three algorithms. As a result of simulation using a random number for the initial phase, the crest factor is about 4; we see that the three algorithms are able to reduce the crest factor. Second, we have investigated sum of cosine waves with initial phases of zero; it would converge to the delta function and it can be for linear system analysis and design. Also we have considered sum of sine waves with initial phases of zero. They are related to the Hilbert transform and complex delta function.

1. Introduction

High quality cosine waves and sine waves are relatively easy to generate electrically and are also useful for theoretical analysis. Therefore, they are widely used for the design and analysis of circuits and systems. In this paper, we investigate the properties of the multi-tone signal (the sum of cosine waves and sine waves of many different frequencies with the same amplitude), and consider its application to design and testing of linear circuits and systems.

In Section 2, we show simulation results of three multi-tone generation algorithms for crest factor reduction. In Section 3, we show simulation results of multi-tone signals with random initial phase. In Section 4, we investigate the properties of the sum of cosine waves with initial phase 0, and show that it converges to the delta function and it can be used for design and analysis of linear system. In Section 5, we investigate the properties of the sum of sine waves with initial phase 0, and show that it converges to $1/(\pi \cdot t)$. In Section 6, the results in Sections 4 and 5 are related to the Hilbert transform. Section 7 provides conclusion.

2. Multi-tone Generation Algorithms for Crest Factor Reduction

In this section, we investigate three multi-tone signal generation algorithms (Kitayoshi, Newman and Schroeder algorithms) and show with simulations that their crest factors are comparable; they are from 1.4 to 2.2 for various numbers of the tones.

The crest factor is defined by the ratio of the peak value of the waveform to the RMS (root-mean-square). If the crest factor of the multi-tone signal is small, each frequency component power can be large for a given full signal range and hence good SNR measurement for each frequency can be obtained simultaneously when the multi-tone signal is applied as an input signal to the analog circuit under measurement. Hence the multi-signal generation is important, especially for the linear circuit and system testing.

2.1 Kitayoshi Algorithm

This subsection shows simulation results of the multi-tone signal generated by the Kitayoshi algorithm in [1]. In equations (1), (2), ϕ_0 is $\pi/2$, the time is from 0 to 8191, and m is 1, 2, 4, 8, 16, 32, 64, 128, 256, 512 or 1024. The simulation results are shown in Fig. 1 (a) to Fig. 11 (a) and their FFT results are shown in Fig. 1 (b) to Fig. 11 (b).

$$\phi_k = \phi_0 - \frac{2\pi}{m}\sum_{j=1}^{k} j \tag{1}$$

$$s(t) = \sum_{j=1}^{m} \sin\left(2\pi \frac{f_j}{N} t + \phi_j\right) \tag{2}$$

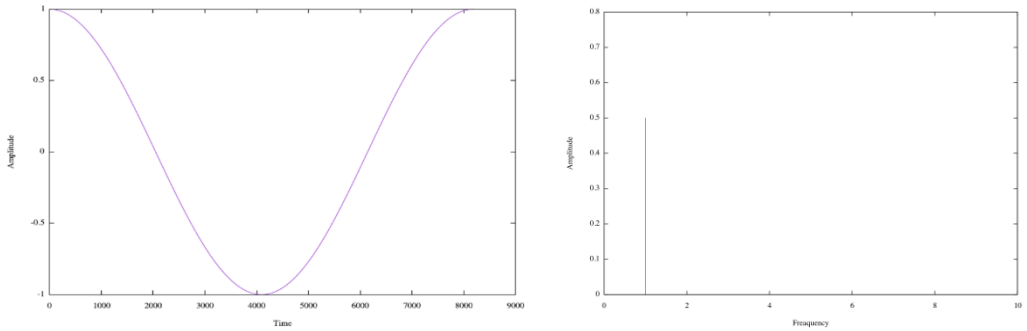

(a) Waveform (Crest factor 1.41) (b) Power spectrum obtained by FFT

Fig. 1. 1-tone signal generated using Kitayoshi algorithm

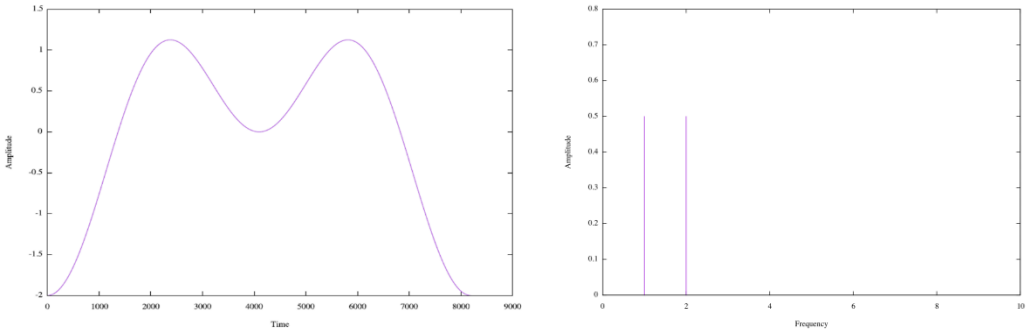

(a) Waveform (Crest factor 2.0) (b) Power spectrum obtained by FFT

Fig. 2. 2-tone signal generated using Kitayoshi algorithm

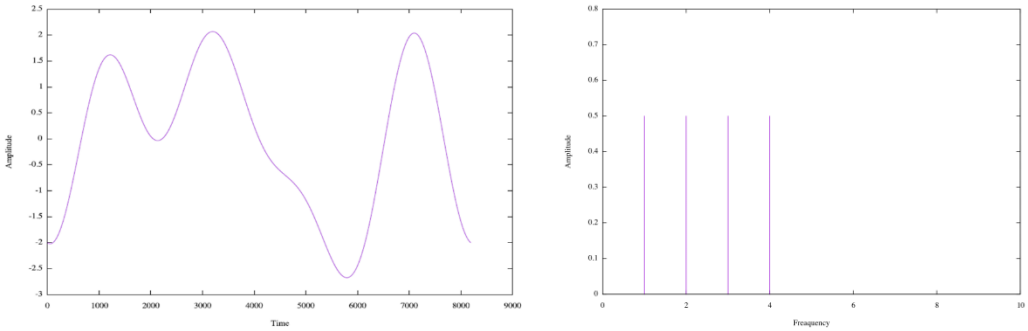

(a) Waveform (Crest factor 1.89) (b) Power spectrum obtained by FFT

Fig. 3. 4-tone signal generated using Kitayoshi algorithm

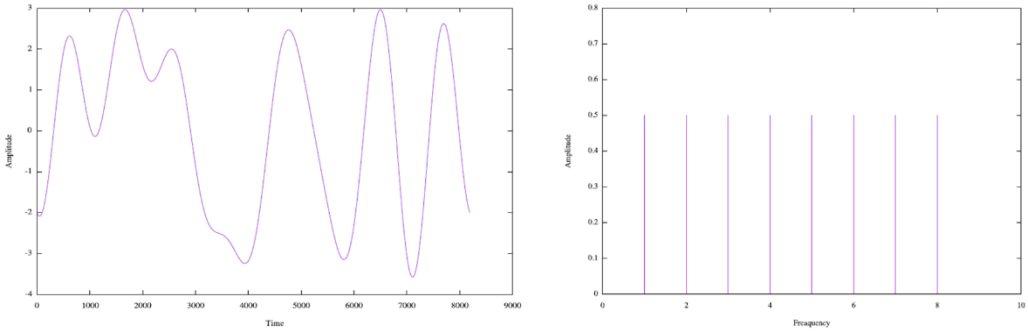

(a) Waveform (Crest factor 1.79) (b) Power spectrum obtained by FFT

Fig. 4. 8-tone signal generated using Kitayoshi algorithm

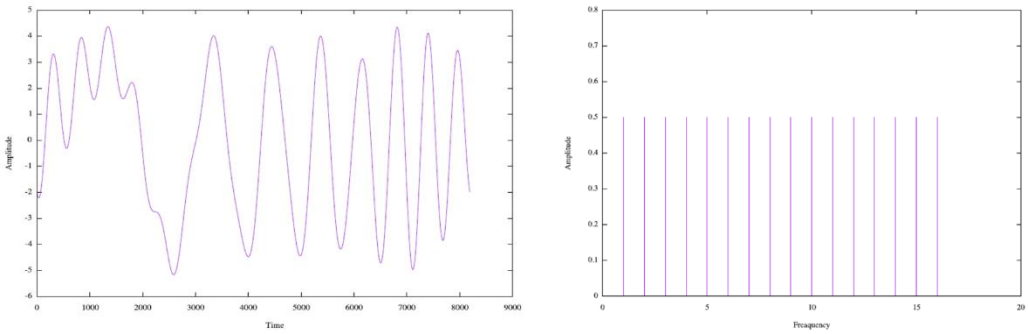

(a) Waveform (Crest factor 1.83) (b) Power spectrum obtained by FFT

Fig. 5. 16-tone signal generated using Kitayoshi algorithm

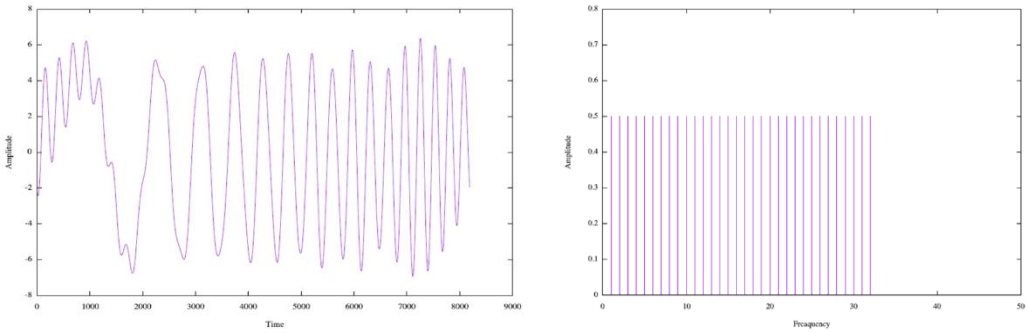

(a) Waveform (Crest factor 1.73) (b) Power spectrum obtained by FFT

Fig. 6. 32-tone signal generated using Kitayoshi algorithm

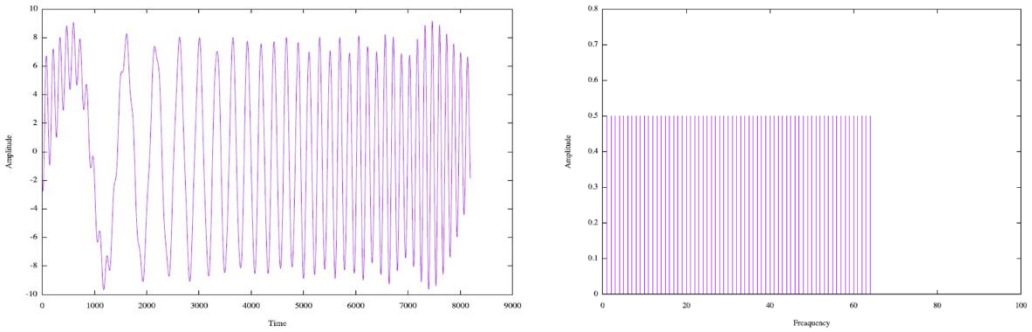

(a) Waveform (Crest factor 1.71) (b) Power spectrum obtained by FFT

Fig. 7. 64-tone signal generated using Kitayoshi algorithm

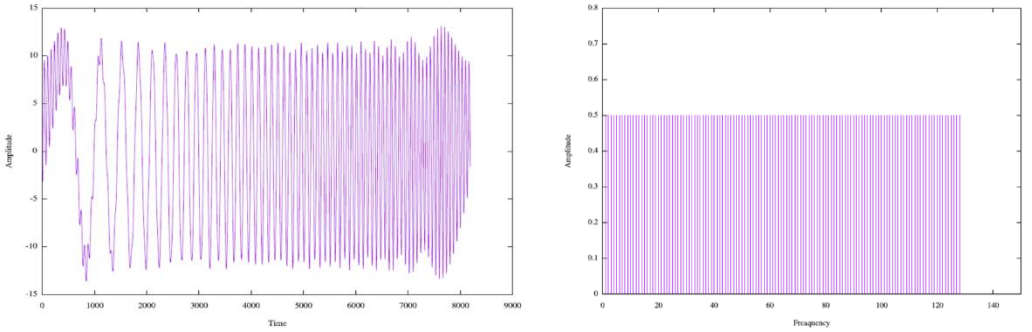

(a) Waveform (Crest factor 1.70) (b) Power spectrum obtained by FFT

Fig. 8. 128-tone signal generated using Kitayoshi algorithm

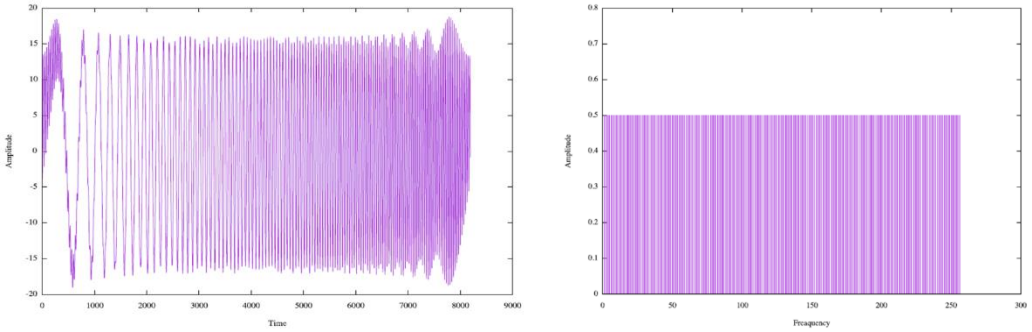

(a) Waveform (Crest factor 1.68) (b) Power spectrum obtained by FFT

Fig. 9. 256-tone signal generated using Kitayoshi algorithm

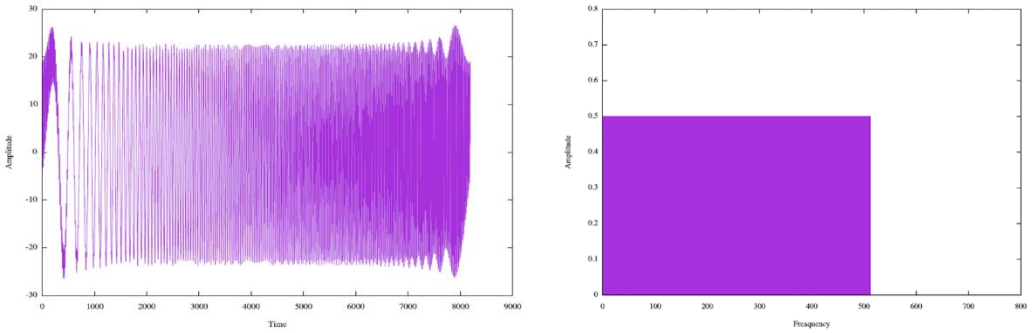

(a) Waveform (Crest factor 1.66) (b) Power spectrum obtained by FFT

Fig. 10. 512-tone signal generated using Kitayoshi algorithm

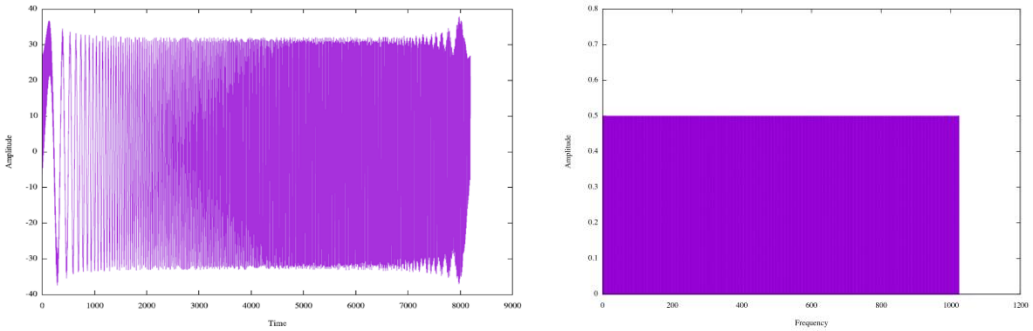

(a) Waveform (Crest factor 1.67) (b) Power spectrum obtained by FFT

Fig. 11. 1024-tone signal generated using Kitayoshi algorithm

Fig. 12 shows the relationship between the number of tones and the crest factor.

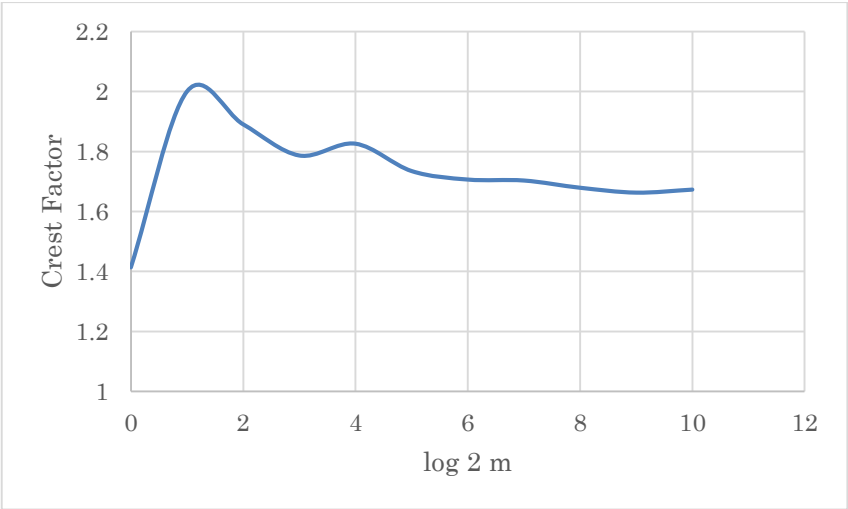

Fig. 12. Relationship between the number of tones and the crest factor for Kitayoshi algorithm

2.2 Newman Algorithm

This subsection shows simulation results of the multi-tone signal generated by the Newman algorithm in [2]. In equations (3), (4), ϕ_0 is $\pi/2$, the time is from 0 to 8191, and m is 2, 4, 8, 16, 32, 64, 128, 256, 512 or 1024. The simulation results are shown in Fig. 13 (a) to Fig. 22 (a) and their FFT results are shown in Fig. 13 (b) to Fig. 22 (b).

$$\phi_k = \frac{\pi(k-1)^2}{m} \tag{3}$$

$$s(t) = \sum_{j=1}^{m} \sin(2\pi \frac{f_j}{N} t + \phi_j) \tag{4}$$

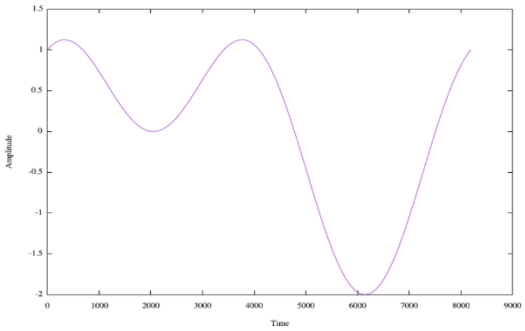

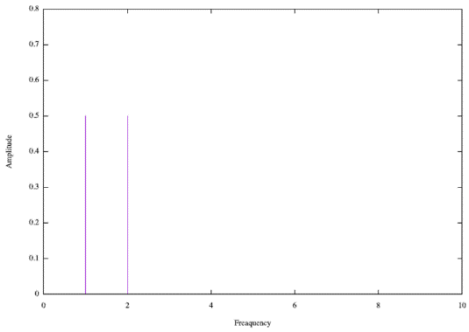

(a) Waveform (Crest factor 2.0) (b) Power spectrum obtained by FFT

Fig. 13. 2-tone signal generated using Newman algorithm

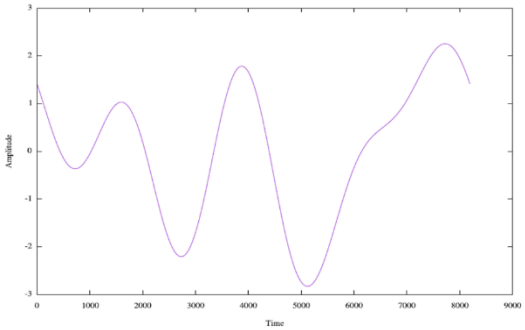

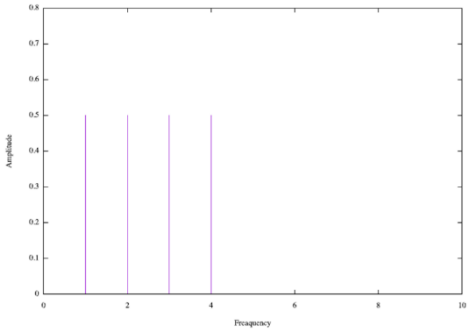

(a) Waveform (Crest factor 2.0) (b) Power spectrum obtained by FFT

Fig. 14. 4-tone signal generated using Newman algorithm

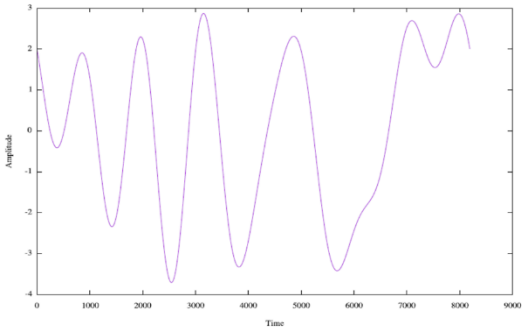

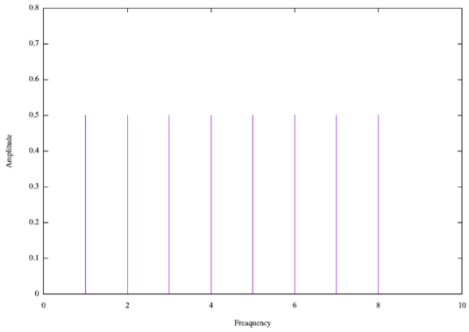

(a) Waveform (Crest factor 1.85) (b) Power spectrum obtained by FFT

Fig. 15. 8-tone signal generated using Newman algorithm

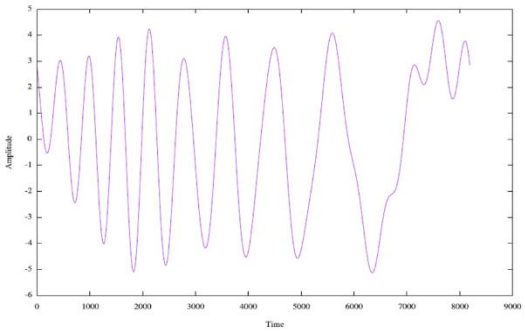

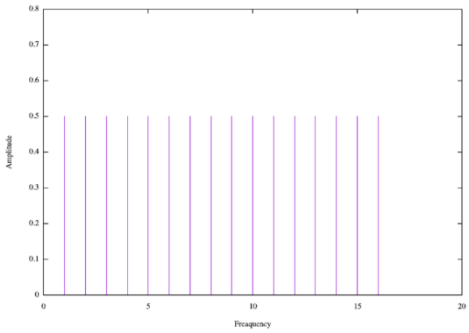

(a) Waveform (Crest factor 1.81) (b) Power spectrum obtained by FF

Fig. 16. 16-tone signal generated using Newman algorithm

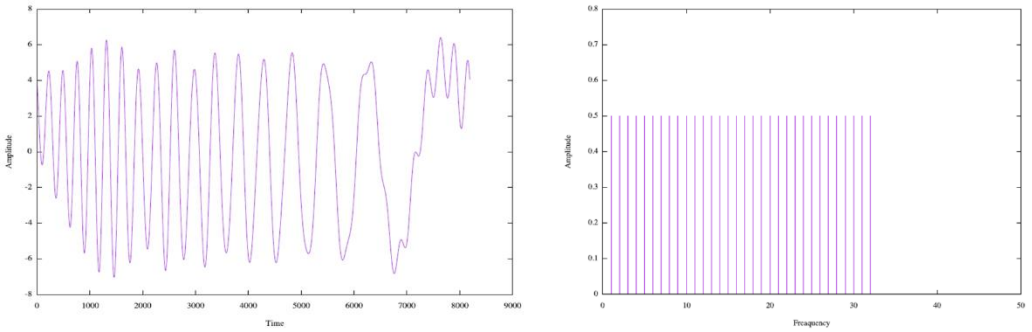

(a) Waveform (Crest factor 1.76) (b) Power spectrum obtained by FFT

Fig. 17. 32-tone signal generated using Newman algorithm

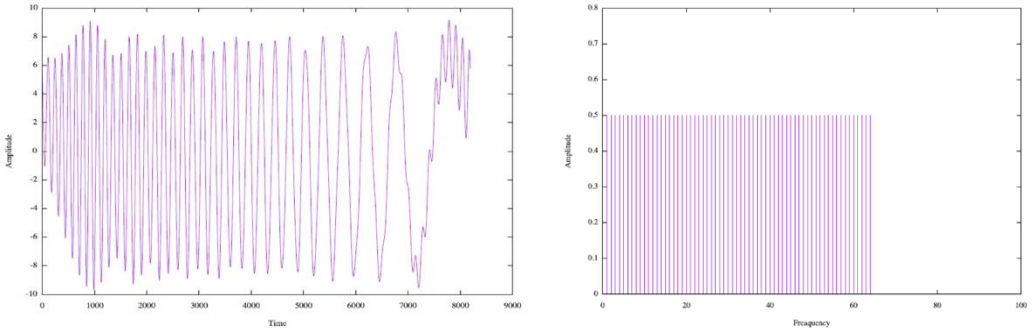

(a) Waveform (Crest factor 1.71) (b) Power spectrum obtained by FFT

Fig. 18. 64-tone signal generated using Newman algorithm

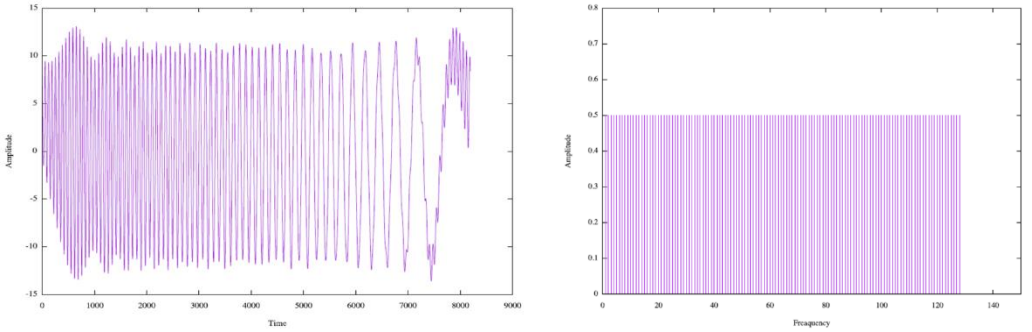

(a) Waveform (Crest factor 1.70) (b) Power spectrum obtained by FFT

Fig. 19. 128-tone signal generated using Newman algorithm

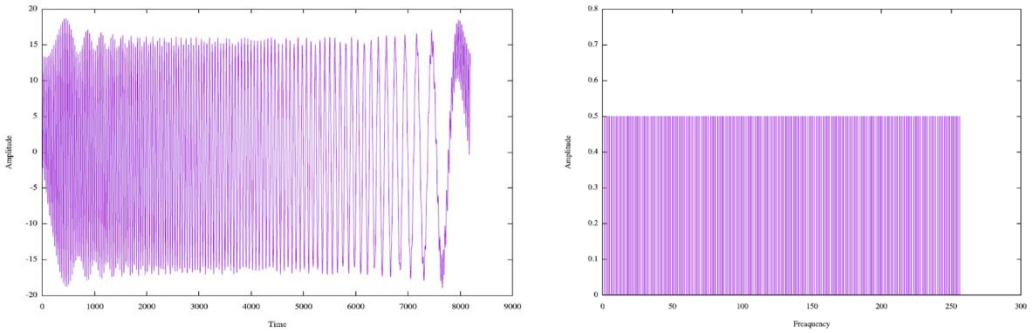

(a) Waveform (Crest factor 1.68) (b) Power spectrum obtained by FFT

Fig. 20. 256-tone signal generated using Newman algorithm

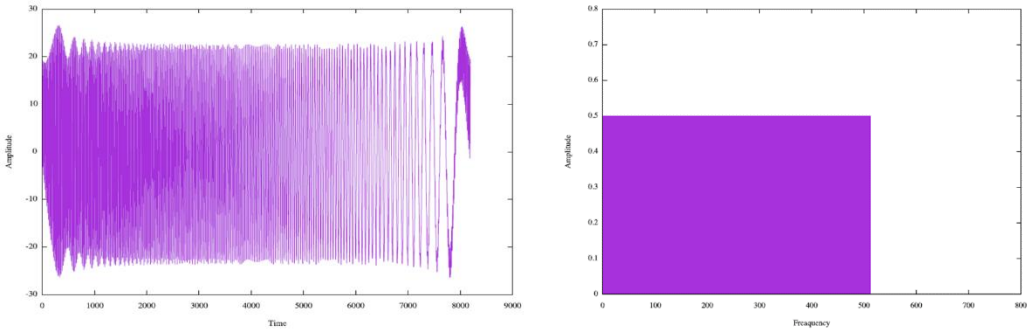

(a) Waveform (Crest factor 1.66) (b) Power spectrum obtained by FFT

Fig. 21. 512-tone signal generated using Newman algorithm

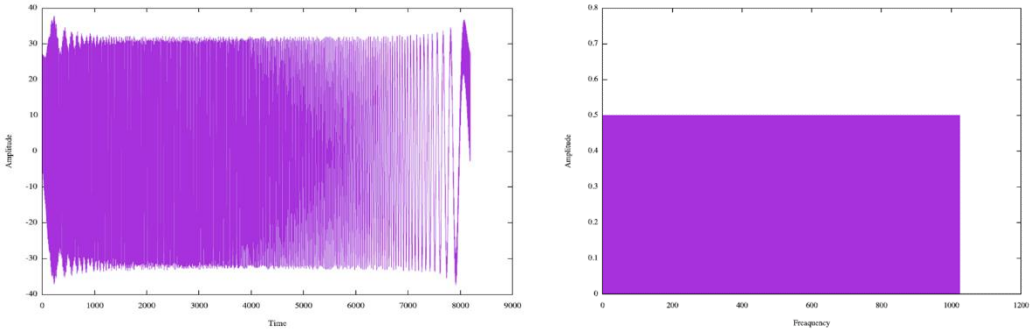

(a) Waveform (Crest factor 1.67) (b) Power spectrum obtained by FFT

Fig. 22. 1024-tone signal generated using Newman algorithm

Fig. 23 shows the relationship between the number of tones and the crest factor.

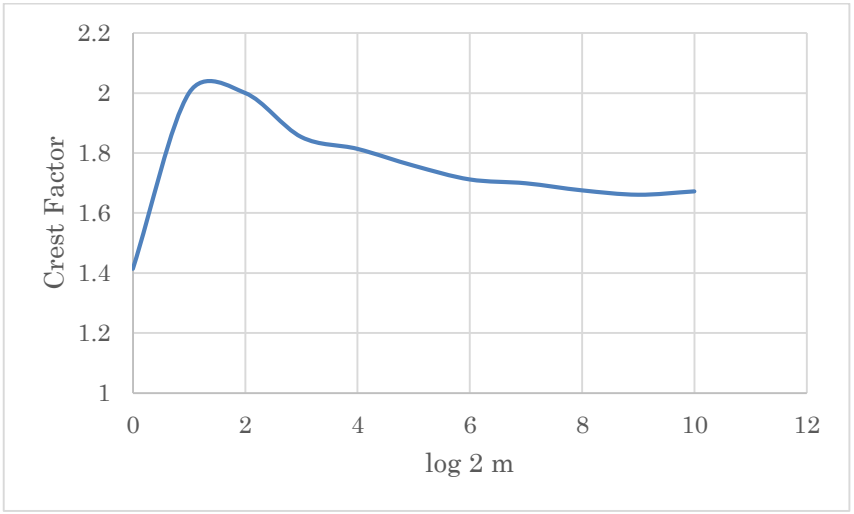

Fig. 23. Relationship between the number of tones and the crest factor for Newman algorithm

2.3 Schroeder Algorithm

This subsection shows simulation results of the multi-tone signal generated by the Schroeder algorithm [3]. In equations (5), (6), ϕ_0 is 0, the time is from 0 to 8191, and m is 2, 4, 8, 16, 32, 64, 128, 256, 512 or 1024. The simulation results are shown in Fig. 24 (a) to Fig. 33 (a) and their FFT results are shown in Fig. 24 (b) to Fig. 33 (b).

$$\phi_k = \phi_1 - \frac{2\pi}{m}\sum_{j=1}^{k-1} jp_j \tag{5}$$

$$s(t) = \sum_{j=1}^{m} \cos(2\pi \frac{f_j}{N} t + \phi_j) \tag{6}$$

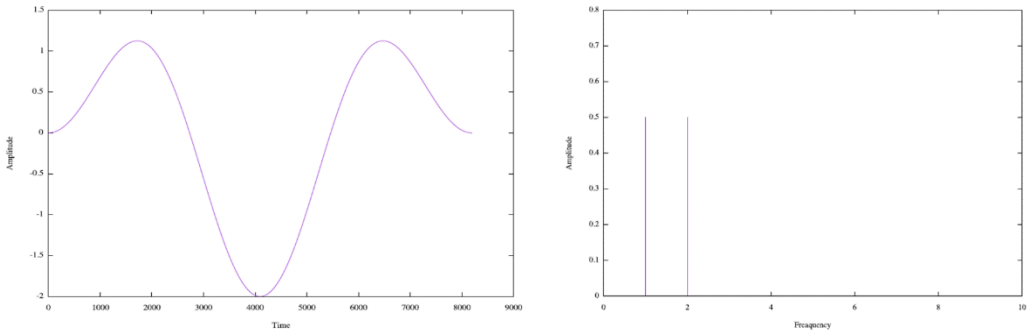

(a) Waveform (Crest factor 2.0) (b) Power spectrum obtained by FFT

Fig. 24. 2-tone signal generated using Schroeder algorithm

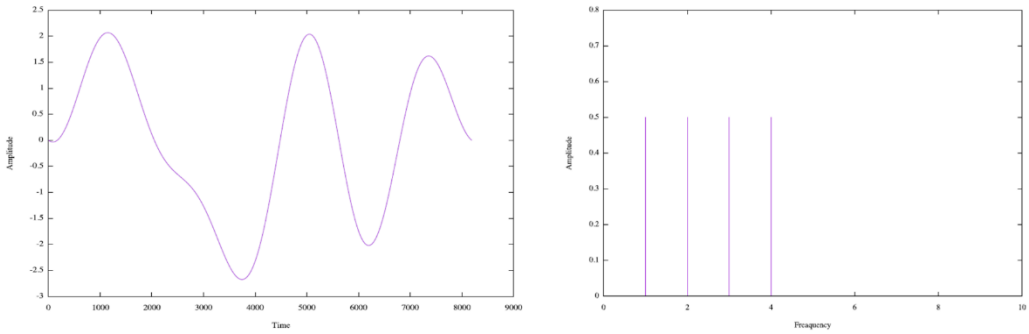

(a) Waveform (Crest factor 1.89) (b) Power spectrum obtained by FFT

Fig. 25. 4-tone signal generated using Schroeder algorithm

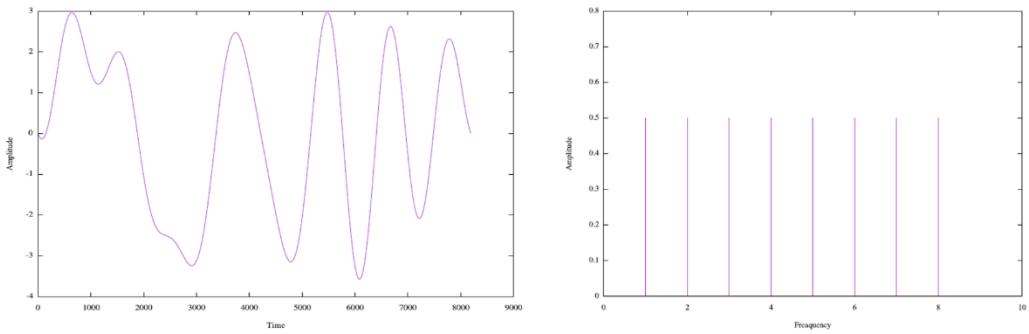

(a) Waveform (Crest factor 1.79) (b) Power spectrum obtained by FFT

Fig. 26. 8-tone signal generated using Schroeder algorithm

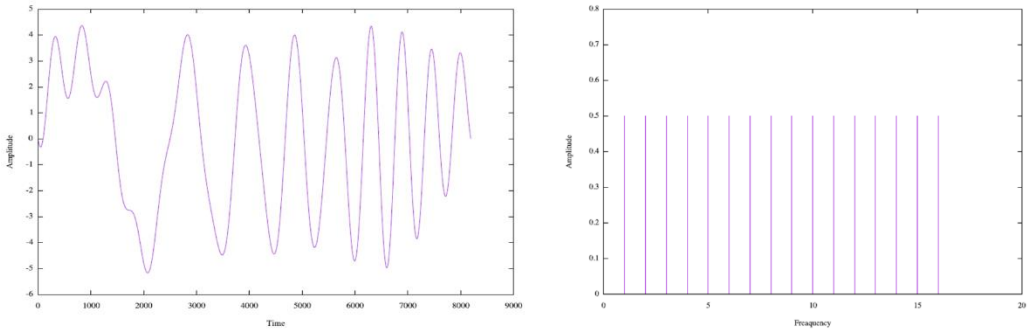

(a) Waveform (Crest factor 1.83) (b) Power spectrum obtained by FFT

Fig. 27. 16-tone signal generated using Schroeder algorithm

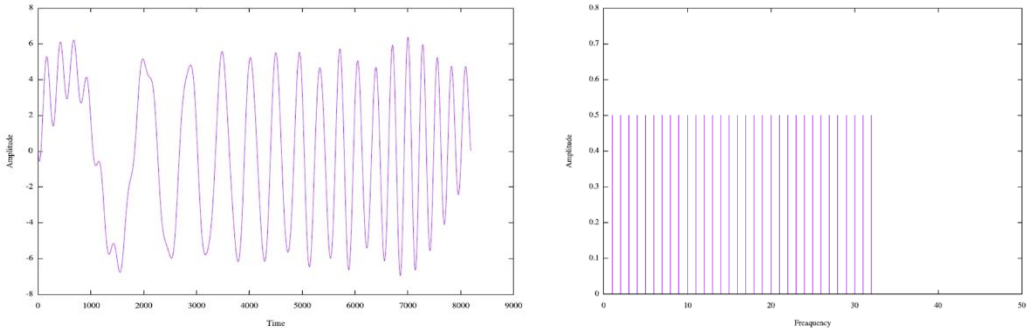

(a) Waveform (Crest factor 1.73) (b) Power spectrum obtained by FFT

Fig. 28. 32-tone signal generated using Schroeder algorithm

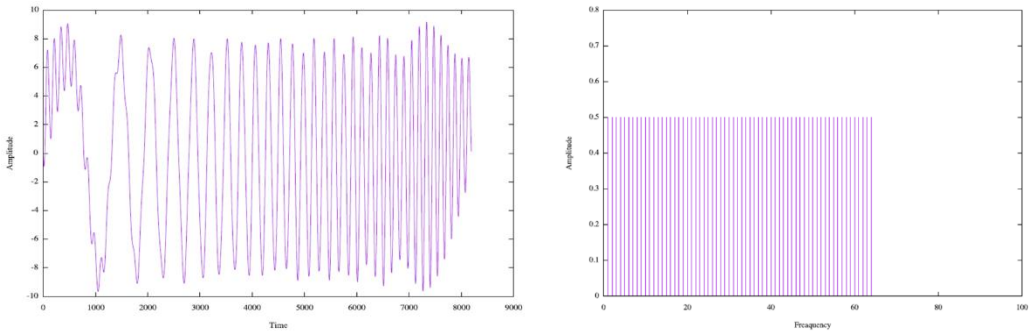

(a) Waveform (Crest factor 1.71) (b) Power spectrum obtained by FFT

Fig. 29. 64-tone signal generated using Schroeder algorithm

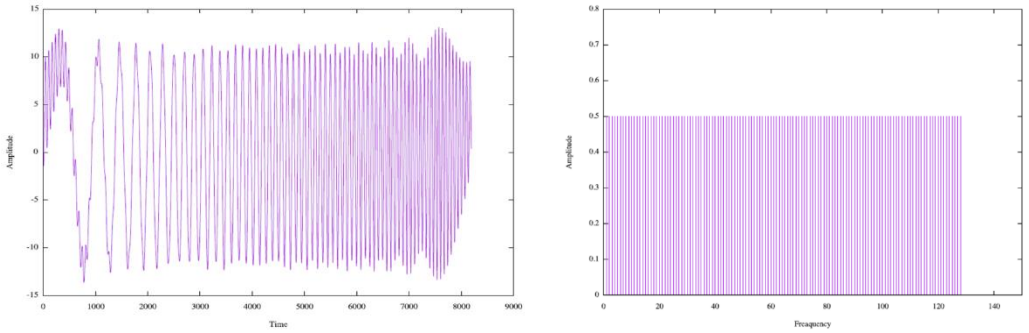

(a) Waveform (Crest factor 1.70) (b) Power spectrum obtained by FFT

Fig. 30. 128-tone signal generated using Schroeder algorithm

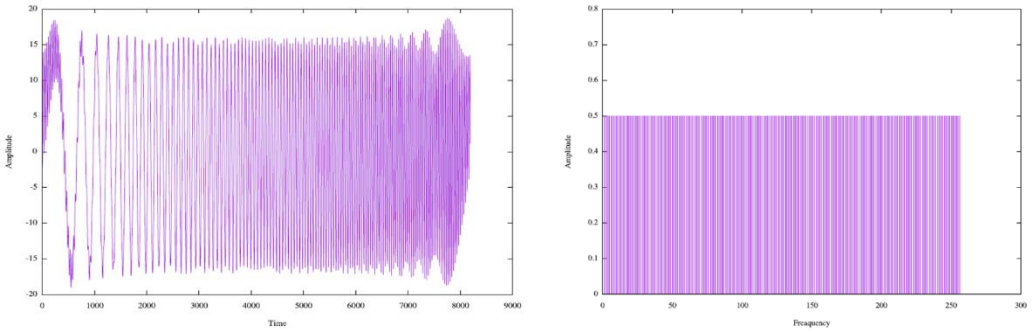

(a) Waveform (Crest factor 1.68) (b) Power spectrum obtained by FFT

Fig. 31. 256-tone signal generated using Schroeder algorithm

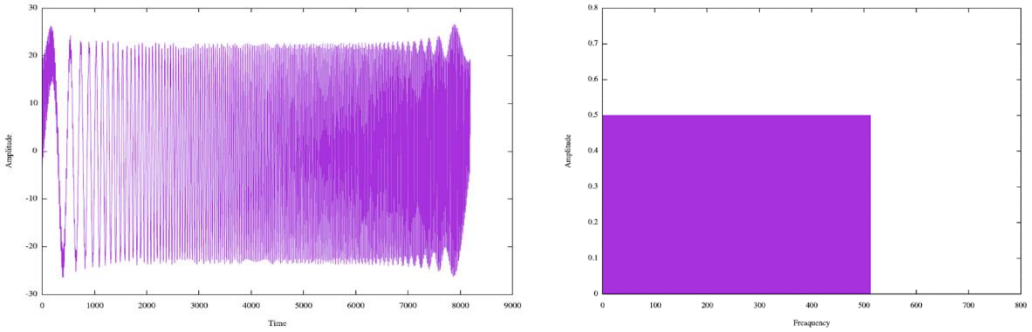

(a) Waveform (Crest factor 1.66) (b) Power spectrum obtained by FFT

Fig. 32. 512-tone signal generated using Schroeder algorithm

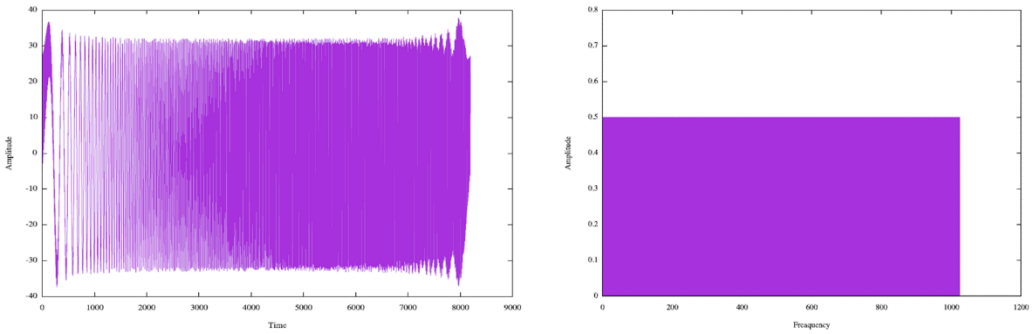

(a) Waveform (Crest factor 1.67) (b) Power spectrum obtained by FFT

Fig. 33. 1024-tone signal generated using Schroeder algorithm

Fig. 34 shows the relationship between the number of tones and the crest factor.

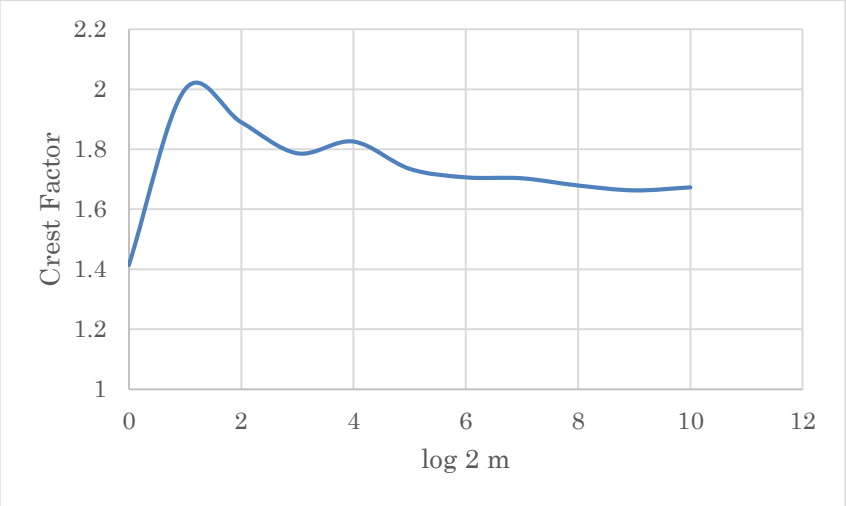

Fig. 34. Relationship between the number of tones and the crest factor for Schroeder algorithm

3. Multi-tone signal with random initial phase

3.1 Sum of cosine waves with random initial phase

We have simulated a multi-cosine signal in equation (7) where each tone has a random initial phase ϕ_j generated as a Gaussian random number. Fig. 35 (b) shows its waveform while Fig. 35 (a) presents its power spectrum obtained by FFT. The crest factor is 4.29, which is 2.5 times larger than that of the above-discussed three algorithms.

$$s(t) = \sum_{j=1}^{m} \cos(2\pi \frac{f_j}{N} t + \phi_j) \quad (7)$$

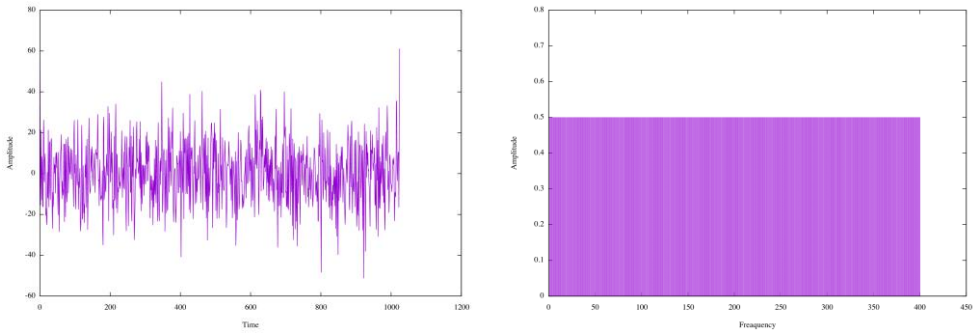

(a) Waveform (Crest factor 4.29) (b) Power spectrum obtained by FFT

Fig. 35. Sum of 400 tone cosine waves with random initial phase

3.2 Sum of sine waves with random initial phase

We have simulated a multi-sine signal in equation (8) where each tone has a random initial phase ϕ_j generated as a Gaussian random number. Fig. 36 (b) shows its waveform while Fig. 36 (a) presents its power spectrum obtained by FFT. The crest factor is 3.39, which is larger than that of the multi-cosine signal.

$$s(t) = \sum_{j=1}^{m} \sin(2\pi \frac{f_j}{N} t + \phi_j) \quad (8)$$

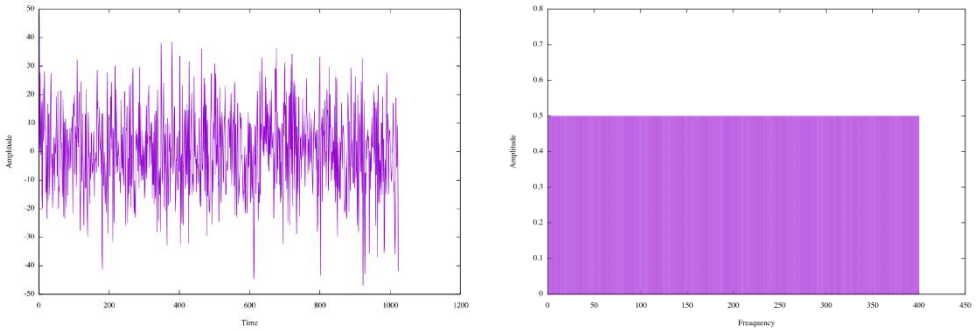

(a) Waveform (Crest factor 3.39) (b) Power spectrum obtained by FFT

Fig. 36. Sum of 400 tone cosine waves with random initial phase

We see from the above results that when using Gaussian random numbers as initial phases, the crest factor becomes larger than when using three algorithms. Therefore, three crest factor reduction algorithms are useful.

4. Sum of cosine waves with zero initial phase

4.1 Sum of cosine waves and delta function

The sum of the cosine waves (phase 0, amplitude 1) of many different frequencies is converges to the impulse signal (delta function), as shown in equation (9).

$$\delta(t) \approx \frac{\omega_o}{2\pi} \sum_{n=-\infty}^{\infty} \cos(n\,\omega_o t) \quad (9)$$

We consider the signal property in the case of addition of finite number 2N + 1 (not infinite number) in equation (10).

$$c(t) = \frac{1}{2N+1} \sum_{n=-N}^{N} \cos(n\,\omega_o t) \quad (10)$$

In the following, we show the results of simulation for equation (11) considering only the positive number n o*f* equation (10).

$$c(t) = \frac{1}{N} \sum_{n=1}^{N} \cos(n\,\omega_o t) \quad (11)$$

Fig. 37 shows the waveform for N = 26, and Fig. 38 shows the one for N = 626.

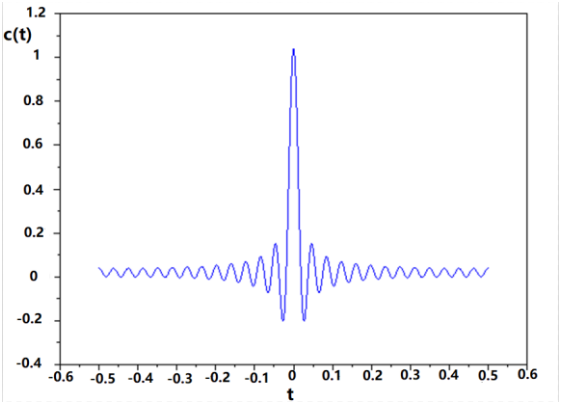

Fig. 37. Sum of N = 26 cosine waves

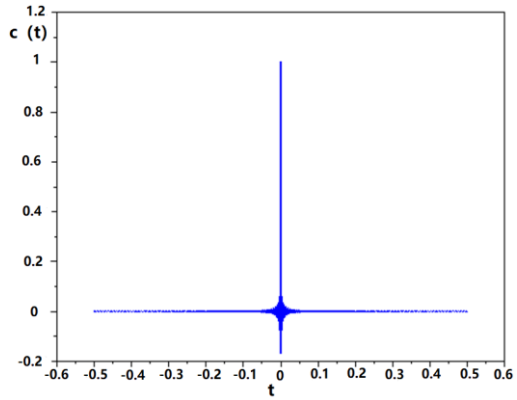

Fig. 38. Sum of N = 626 cosine waves

$$d(t) = (2N + 1) \cdot c(t) = \sum_{n=-N}^{N} \cos(n\,\omega_o t) \qquad (12)$$

We can estimate that d(0) = 2N + 1 converges to a delta function. Strictly speaking, since d (t) is the sum of discrete frequencies, it is a periodic delta function, though.

4.2 Relationship between the number of cosine waves and full width at half maximum

Fig. 39 shows the definition of full width at half maximum (FWHM) W.

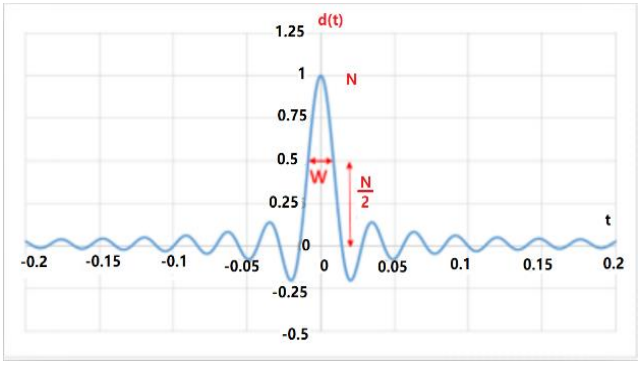

Fig. 39. Definition of full width at half maximum W

Fig. 40 shows the relationship between W and $1/N$ obtained by numerical calculation. We see that W and $1/N$ are proportional.

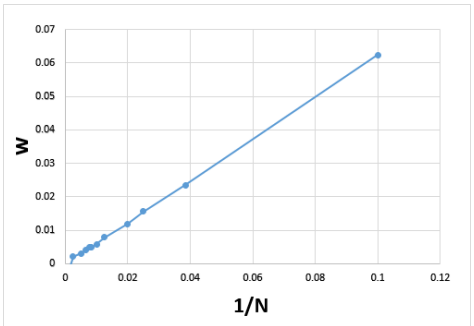

Fig. 40. Relationship between W and $1/N$

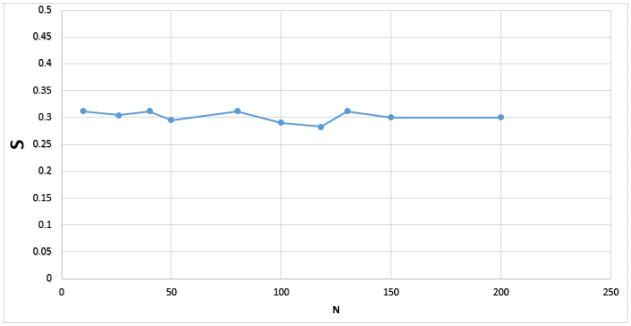

Fig. 41. Relationship between S and N

The area of the impulse portion of d(t) is approximated to $(1/2)N \cdot W$ in Fig.40. Fig. 41 shows the relationship between this approximated area ($(1/2)N \cdot W$) and N, while Fig. 42 shows the

relationship between $s \cdot \pi$ and N. It turns out that the area becomes $1/\pi$ regardless of N. This can be explained by the uncertainty relationship between the frequency and the time. For any signal, if its spread in the frequency domain is narrow, its spread of the time domain has to be wide, and both cannot be narrow simultaneously. [6, 7]

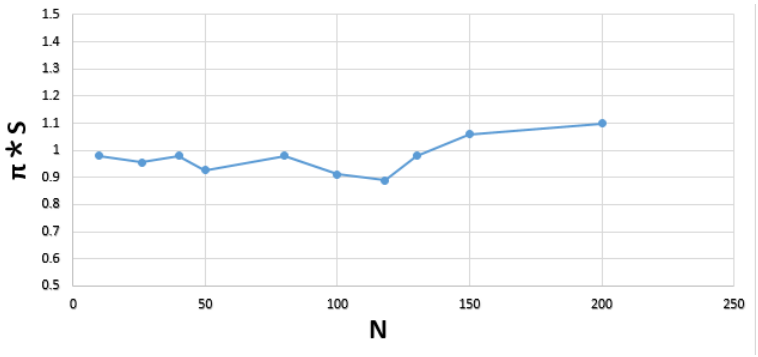

Fig. 42. Relationship between $s \cdot \pi$ and N

4.3 Application of the sum of cosine waves to circuit system design and analysis

- The finite number of sum for cosine waves can be used to design the digital filter coefficients of the Mexican hat filter by choosing an appropriate N.
- A sharp impulse signal used for the impulse sampling clock of the wideband sample and hold circuit can be realized with the sum of the cosine waves with initial phases of zero in equation (12).
- Equation (12) explains that a sharp impulse signal has wideband characteristics or UWB (Ultra Wide Band).
- The theorem that in a linear time-invariant system, the Fourier transform of its impulse response is its frequency transfer function can be proved using equation (12).
- There is some possibility that a calculation formula can be derived in the form of series expansion of π from the fact that the area of d(t) is approximated to π.

5. Sum of sine waves with zero initial phase

5.1 Sum of sine waves and convergence to $1/(\pi \cdot t)$

We consider the nature of the signal in the case of addition of a finite number N of many different frequency sine waves (phase 0, amplitude 1) of the equation (13).

$$s(t) = \sum_{n=1}^{N} \sin(n\,\omega_o t) \tag{13}$$

Fig. 43 shows N = 38, and Fig. 44 shows N = 198. s(t) converges to $1/(\pi \cdot t)$. Fig. 45 and Fig. 46 show the relationship between s (t) and $1/(\pi \cdot t)$ obtained by numerical calculation when N = 198 and N = 298. s(t) and $1/(\pi \cdot t)$ are almost equal.

A new mathematical formula can be derived from Figs. 45, 46. Notice

$$\frac{1}{2\pi t} = \int_0^\infty \sin(\omega t) d\omega$$

and then, we obtain the following formula:

$$\frac{\ln(t)}{2\pi} = -\int_0^\infty \frac{1}{\omega} \cos(\omega t) d\omega + C$$

Here C is constant. This formula may be useful when cos(ωt)/(ωt) is used for design and analysis of linear systems and circuits.

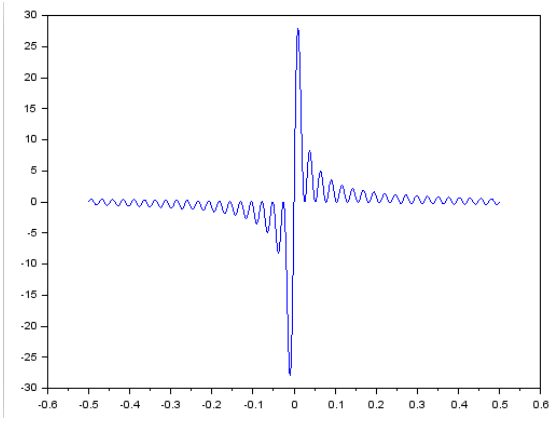

Fig. 43. Sum of N = 38 sine waves

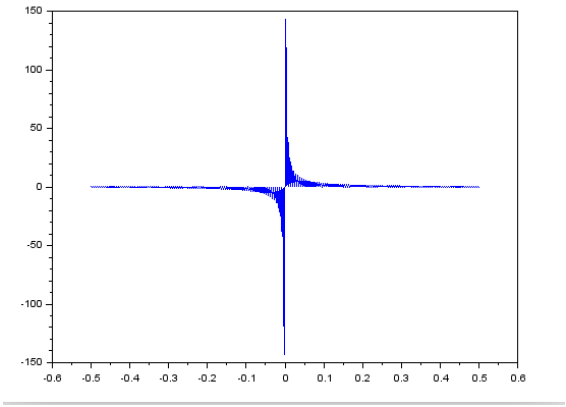

Fig. 44. Sum of N = 198 sine waves

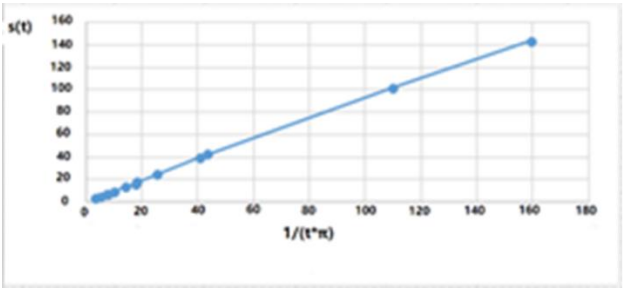

Fig. 45. Relationship at N = 198

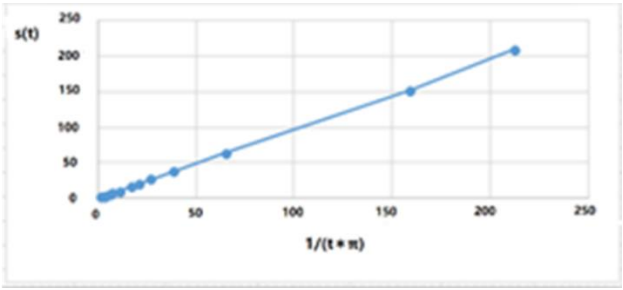

Fig. 46. Relationship at N = 298

6. Application of the sum of cosine waves and sine wave to circuit system design and analysis

- We can implement complex (quadrature) impulse signal by setting the real part signal as the sum of cosine waves and the imaginary part signal as the sum of the sine waves. (Fig. 47, [4])
- Some researchers pointed out that there is a practical problem in high-speed processing because Hilbert transformation has a long impulse response.
- By inputting these signals in the complex signal circuit, we can obtain its complex impulse response. (Fig. 48, [5])

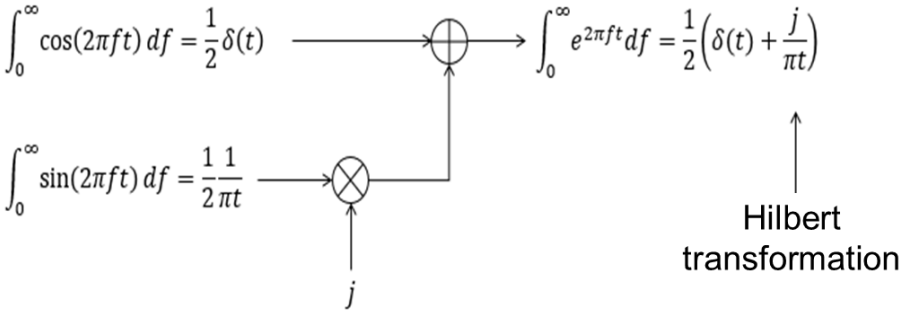

Fig. 47. Complex impulse signal and Hilbert transformation

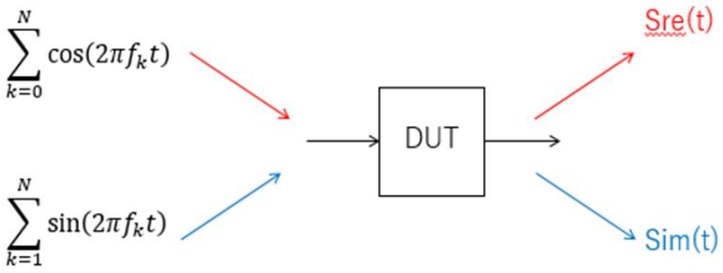

Fig. 48. Impulse response measurement of complex signal circuit

7. Conclusion

In this paper, we have compared three algorithms to reduce the crest factor of multi-tone signals. Comparing the simulation results, it is found that the crest factor when the initial phase is properly set using the algorithm is about 1.8, while the crest factor when the initial phase is a random number is 4. Therefore, it turned out that three algorithms (especially Schroeder) are useful. In addition, the properties of the multi-tone signal (the signal of the sum of cosine waves and sine waves of many different frequencies with the same amplitude) were investigated and the application to design, analysis and testing of the linear circuits and systems was examined.

References

[1] H. Kitayoshi, S. Sumida, K. Shirakawa and S. Takeshita, “DSP Synthesized Signal Source for Analog Testing Stimulus and New Test Method”, IEEE International Test Conference, pp.825-834, 1985.

[2] D. J. Newman, “An L1 Extremal Problem for Polynomials”, Proc. of the American Mathematics Society, vol. 16, pp. 1287-1290, Dec. 1965.

[3] M. R. Schroeder, “Synthesis of Low-Peak-Factor Signals and Binary Sequences with Low Autocorrelation”, IEEE Trans. Information Theory, pp.85-89, 1970.

[4] Y. Tamura, R. Sekiyama, K. Asami, H. Kobayashi, "RC Polyphase Filter As Complex Analog Hilbert Filter", IEEE 13th International Conference on Solid-State and Integrated Circuit Technology, Hangzhou, China (Oct. 2016).

[5] T. J. Yamaguchi, M. Soma, M. Ishida, T. Watanabe, T. Ohmi, “Extraction of Instantaneous and RMS Sinusoidal Jitter Using an Analytic Signal Method,” IEEE Trans. Circuits and Systems- II (June 2003).

[6] L. Cohen, Time-Frequency Analysis: Their Applications, Printice-Hall (1994)

[7] H. Kobayashi, I. Shimizu, N. Tsukiji, M. Arai, K. Kubo, H. Aoki ,"Fundamental Design Tradeoff and Performance Limitation of Electronic Circuits Based on Uncertainty Relationships,” IEEE 12th International Conference on ASIC, Guiyang, China (Oct, 2017).